NJC

ROYAL SOCIETY OF CHEMISTRY

PAPER

View Article Online
View Journal | View Issue

Cite this: *New J. Chem.*, 2020, **44**, 8241

Ultrastable conductive microporous covalent triazine frameworks based on pyrene moieties provide high-performance CO_2 uptake and supercapacitance†

Mohamed Gamal Mohamed, [ab] Ahmed F. M. EL-Mahdy, [ab] Yasuno Takashi[a] and Shiao-Wei Kuo *[ac]

Received 15th March 2020,
Accepted 30th April 2020

DOI: 10.1039/d0nj01292k

rsc.li/njc

Covalent organic triazine frameworks (CTFs) are a subclass of covalent organic frameworks and conjugated microporous polymers that exhibit heteroatom effects and possess high surface areas and excellent chemical and thermal stabilities; they have applications in energy storage and gas adsorption. In this study, we prepared two microporous polymers the pyrene-functionalized CTFs Pyrene-CTF-10 and Pyrene-CTF-20—through ionothermal treatment of 1,3,6,8-cyanopyrene (TCNPy) in the presence of molten zinc chloride ($ZnCl_2$) at 500 °C (at $ZnCl_2$-to-TCNPy molar ratios of 10 : 1 and 20 : 1, respectively). Pyrene-CTF-10 and Pyrene-CTF-20 had specific BET surface areas of 819 and 1019 $m^2\ g^{-1}$, respectively, with pore size distributions of 1.10 and 1.35 nm, respectively, and high char yields (up to 70%). Furthermore, these Pyrene-CTF polymeric frameworks exhibited excellent specific capacitances at a current density of 0.5 A g^{-1}: 380 F g^{-1} for Pyrene-CTF-10 and 500 F g^{-1} for Pyrene-CTF-20. In addition, both Pyrene-CTFs had excellent cycling stability, retaining 97% of their capacitances after cycling 2000 times at a current density of 10 A g^{-1}. Moreover, Pyrene-CTF-10 displayed good CO_2 uptake capacity (2.82 and 5.10 mmol g^{-1} at 298 and 273 K, respectively).

Introduction

Supercapacitors, also known as electrochemical capacitors or electric double-layer capacitors (EDLCs), are being used more widely as replacements for fuel cells and batteries in energy storage applications, military devices, electric vehicles, and electrochemical devices because of their long lifetimes, rapid rates of charging and discharging, and high power densities.[1,2] The electrochemical mechanisms behind the operation of supercapacitors can be divided into two categories: nonfaradaic processes (*e.g.*, in EDLCs) depending on the accumulation of electrostatic charge at the electrode–electrolyte interface and faradaic processes (*e.g.*, in pseudocapacitors) occurring at the surfaces of conjugated polymers, heteroatom-doped carbon materials, and metal oxide/hydroxide systems that feature fast redox reactions.[2,3] Thus, the construction of materials for use as electrodes in energy storage applications requires that they have large specific surface areas, high nitrogen contents, large surface areas available to the electrolyte, and hierarchical porous structures.[3–5] Anthropogenic carbon dioxide (CO_2) emissions will likely have many serious negative effects on human life and the environment because of increasing global temperatures and changes to weather events.[6–9] Therefore, lowering emissions and the levels of CO_2 through sequestration and capture has become a challenge for both academia and industry. The wet cleaning method has been the most commonly used chemical process for capturing and separating CO_2 with aqueous alkanolamine solutions (amine scrubbing), but this method has the disadvantages of high energy consumption, low efficiency, difficulties of renewal, amine-mediated corrosion of equipment, solvent loss, and high cost.[10–15] As a result, we need new and effective methods for decreasing the emission and increasing the capture of CO_2 during industrial processes. Covalent organic polymers (COPs) are attractive porous materials for many applications, including sensors; the removal of pollutants; CO_2 capture, storage, and separation; drug delivery; catalysis; SO_2 adsorption; gene therapy; Li–S batteries; energy conversion; and light-harvesting. They have many interesting properties: outstanding thermal stability, high BET surface areas, accessible porosity, large pore volumes,

[a] *Department of Materials and Optoelectronic Science, Center of Crystal Research, National Sun Yat-Sen University, Kaohsiung, Taiwan. E-mail: kuosw@faculty.nsysu.edu.tw*
[b] *Chemistry Department, Faculty of Science, Assiut University, Assiut, 71516, Egypt*
[c] *Department of Medicinal and Applied Chemistry, Kaohsiung Medical University, Kaohsiung, 807, Taiwan*

† Electronic supplementary information (ESI) available. See DOI: 10.1039/d0nj01292k

chemical resistance, biocompatibility, and excellent electrical conductivity when compared with metal–organic frameworks.[16–26] The many types of COP materials include covalent organic frameworks (COFs), covalent triazine frameworks (CTFs), porous aromatic frameworks, benzimidazole-linked polymers, carbazole-based microporous polymers, and porous imine-linked networks.[27–34] Amine scrubbing adsorbs CO_2 through chemisorption, as opposed to the physisorption mechanism of COPs.[10,12,34] Post-synthesis or bottom-up approaches can be used to incorporate CO_2-philic functional groups [*e.g.*, carboxyl (COOH), hydroxyl (OH), imine (–N═CH), benzimidazole, carbazole, and triazine units] into covalent organic porous materials to improve their CO_2 capture.[34–38] CTFs are both COFs and conjugated microporous polymers that display large heteroatom effects, possess permanent nanopores with high Brunauer–Emmett–Teller (BET) surface areas, have excellent chemical and thermal stabilities, and feature tunable electronic structures.[39–43] Most CTF framework materials have been prepared through ionothermal trimerization of nitrile groups, superacid catalysis, and phosphorous pentoxide (P_2O_5) catalysis.[28,43–45] Many recent reviews have highlighted the great potential of CTF materials in gas separation and storage, heterogeneous catalysis, energy storage, and photocatalysis.[46–48] Porous polymeric materials containing pyrene units have been tested recently in many different fields—including chemical sensing, photoelectric devices, gas storage and separation, and photocatalysis—because of their high propensity for forming excimers, distinct solvatochromic phenomena, ready functionalization, delayed fluorescence, and tunable photophysical properties.[49–51]

In a previous study, we prepared a series of conductive bicarbazole-based CTFs (Car-CTFs) through the trimerization of [9,9′-bicarbazole]-3,3′,6,6′-tetracarbonitrile (Car-4CN) with molten zinc chloride ($ZnCl_2$); these materials exhibited outstanding thermal stability, excellent energy storage, and CO_2 uptake.[28] Janiak *et al.* prepared the CTFs PCTF-1 and PCTF-2 through reactions of tetra(4-cyanophenyl)ethylene with $ZnCl_2$ at 400 °C; these two materials captured CO_2 at levels of 3.30 and 1.87 mmol g^{-1}, respectively, at 273 K.[52] Voort *et al.* prepared CTF materials from 4,4′,4″,4‴-(1,4-phenylenebis(pyridine-4,2,6-triyl))tetrabenzonitrile in anhydrous $ZnCl_2$ under ionothermal conditions at 400 and 500 °C, with the former material (CTF-20-400) providing a CO_2 uptake of 3.48 mmol g^{-1} at 273 K.[8] Han *et al.* prepared the CTF TPC-1 through defluorination carbonization and trimerization of the nitrile groups of tetrafluoroterephthalonitrile in molten $ZnCl_2$; this polymeric framework had a high specific surface area (1940 m^2 g^{-1}) and displayed

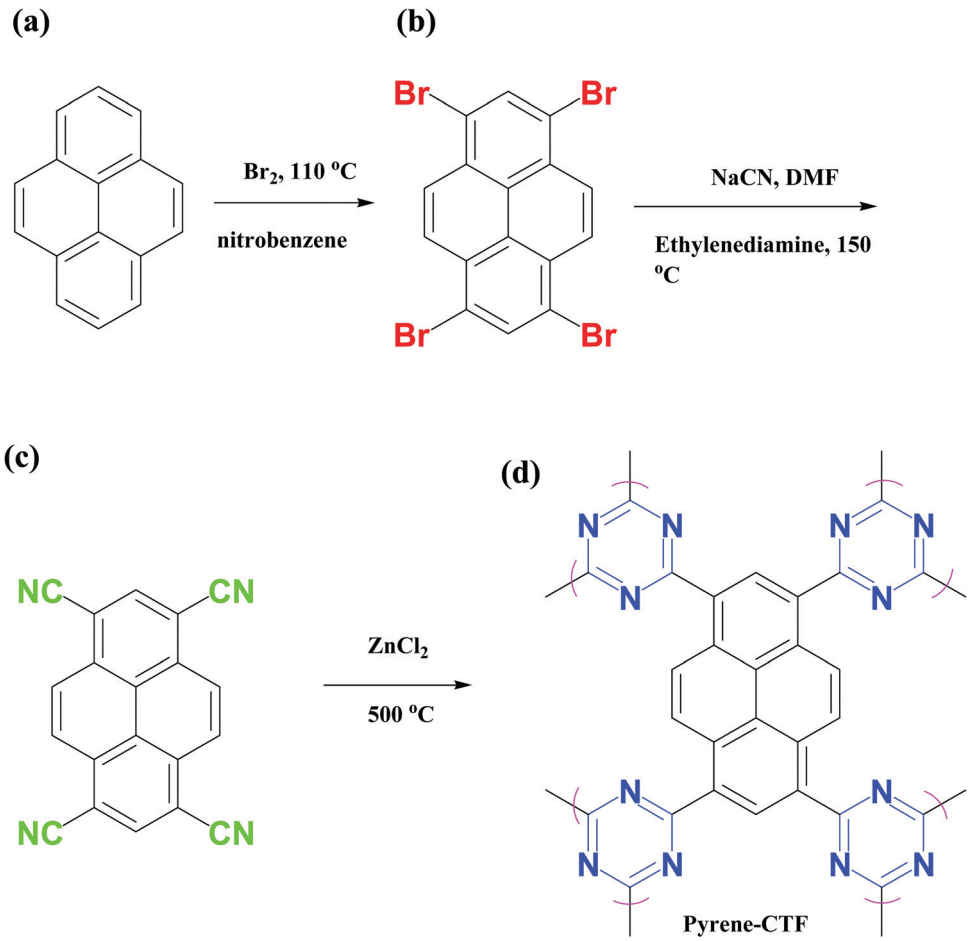

Scheme 1 Synthesis of (d) Pyrene-CTF from (a) pyrene, (b) TBrPy, and (c) TCNPy.

excellent CO_2 adsorption (4.9 mmol g^{-1} at 273 K). In this study, we prepared pyrene-based CTFs (Pyrene-CTFs) through trimerization of the nitrile groups of 1,3,6,8-cyanopyrene (TCNPy) in the presence of molten $ZnCl_2$ at 500 °C (Scheme 1). We used wide-angle X-ray diffraction (WAXD), Fourier transform infrared (FTIR) spectroscopy, X-ray photoelectron spectroscopy (XPS), Raman spectroscopy, transmission electron microscopy (TEM), thermogravimetric analysis (TGA), and the Brunauer–Emmett–Teller (BET) method to examine the properties of these Pyrene-CTFs (crystallinity BET surface areas, porosities, chemical surface compositions, thermal stability, and chemical structures). We performed electrochemical measurements and CO_2 uptake analyses to examine their potential applications as high-performance electrode materials and for gas adsorption.

Experimental section

Materials

Pyrene, nitrobenzene, HCl solution (37%), ethanol (EtOH), and methanol (MeOH) were purchased from Acros. Ethylenediamine (99%), tetrahydrofuran (THF), *N*,*N*-dimethylformamide (DMF), dichloromethane (DCM), acetone, and copper(I) cyanide (CuCN) was purchased from Sigma-Aldrich.

1,3,6,8-Tetrabromopyrene (TBrPy)[54,55]

A solution of bromine (1.15 mL, 22 mmol) in nitrobenzene (5 mL) was added dropwise to a solution of pyrene (1 g) in nitrobenzene (15 mL) and then the mixture was heated at 120 °C for 4 h. Cooling to room temperature provided a pale-green solid, which was filtered off, washed three times with EtOH, and dried under vacuum at 100 °C to provide a pale-green solid (2.21 g, 91%). M.p.: >300 °C.

1,3,6,8-Cyanopyrene (TCNPy)

A mixture of TBrPy (3.00 g, 4.65 mmol) and CuCN (9.69, 108 mmol) in dry DMF (100 mL) was heated under reflux under a N_2 atmosphere at 140 °C for 3 days. The mixture was opened to the air and cooled to room temperature, at which point it was then filtrated to remove unreacted CuCN. The solution was poured into a mixture of cold water (75 mL) and ethylenediamine (4 mL); this mixture was heated at 50 °C

Table 1 Thermal stabilities, porosity parameters, Raman spectral data, and electrochemical data of the Pyrene-CTFs

Sample	TCNPy/$ZnCl_2$	$T_{d10\%}$ (°C)	Char yield (%)	S_{BET} (m^2 g^{-1})	Pore size (nm)	Pore volume (cm^3 g^{-1})	I_D/I_G (Raman)	CV (F g^{-1})
Pyrene CTF-10	1 : 10	500	72	819	1.10	0.88	1.07	380
Pyrene-CTF-20	1 : 20	474	72	1019	1.35	1.12	1.47	500

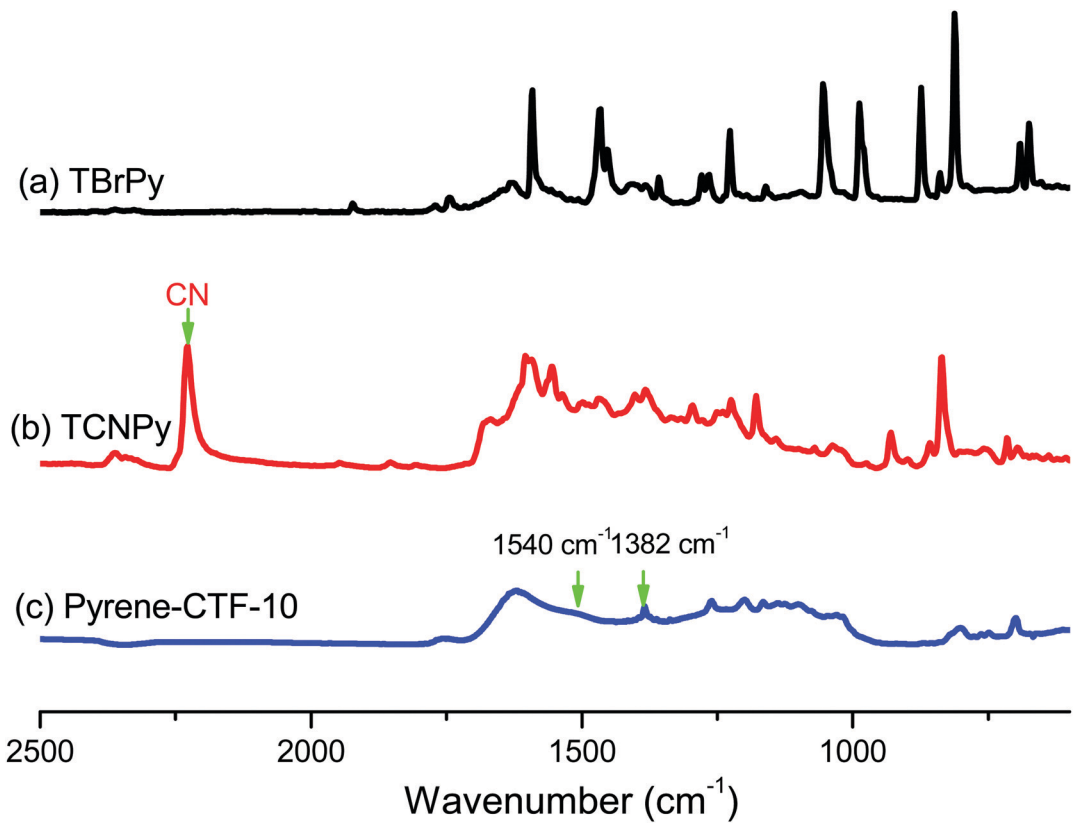

Fig. 1 FTIR spectra of (a) TBrPy, (b) TCNPy, and (c) Pyrene-CTF-10.

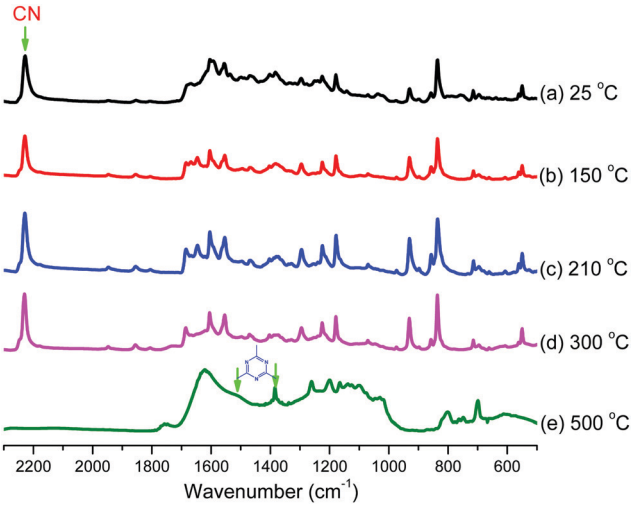

Fig. 2 FTIR spectral profile of Pyrene-CTF-10, recorded at temperatures from room temperature to 500 °C.

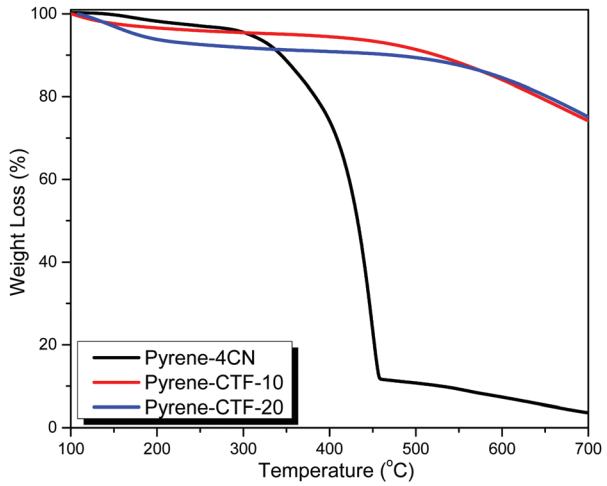

Fig. 3 TGA analyses of TCNPy, Pyrene-CTF-10, and Pyrene-CTF-20, recorded under N_2.

for 2 h. The yellow powder was filtered off and washed with water and MeOH to afford a yellow powder (1.24 g). M.p.: >400 °C; FTIR (KBr, cm^{-1}): 3070 (C–H stretching), 2220 (CN stretching).

Pyrene-CTFs

In an ampoule, TCNPy (200 mg, 0.46 mmol) was mixed with anhydrous $ZnCl_2$ [63 mg (4.63 mmol) or 126 mg (9.26 mmol)] (Scheme 1). The temperature was raised to 500 °C at a heating rate of 5 °C min^{-1} and then the samples were maintained at that temperature for 48 h under the N_2 atmosphere. After cooling, each obtained black solid was washed with 1 M HCl and water (each for 24 h). The resultant black solids (Py-CTF-10, Py-CTF-20) were washed several times with THF, DCM, and MeOH. Finally, the black powders were dried for 24 h at 100 °C.

Results and discussion

Synthesis of TBrPy, TCNPy, and Pyrene-CTFs

The monomer 1,3,6,8-cyanopyrene (TCNPy) was synthesized in two steps (Scheme 1). First, pyrene was reacted with bromine (Br_2) in nitrobenzene at 120 °C for 5 h to afford TBrPy as a pale-green solid, which was reacted with CuCN in DMF at 140 °C for 48 h to give TCNPy as a yellow powder. We then used an ionothermal method for trimerization of the nitrile groups of TCNPy in the presence of molten anhydrous $ZnCl_2$ (at weight ratios of 1 : 10 and 1 : 20) at 500 °C to give Pyrene-CTF-20 and Pyrene-CTF-20, respectively (Scheme 1 and Table 1). Fig. 1 displays the FTIR spectra of TBrPy, TCNPy, and the Pyrene-CTFs. The spectrum of TBrPy [Fig. 1(a)] featured characteristic absorption bands centered at 3050 and 804 cm^{-1}, assigned to the stretching of aromatic C–H[56–59] and C–Br bonds, respectively. The FTIR spectrum of TCNPy [Fig. 1(b)] contained an absorption band at 2220 cm^{-1} representing the stretching of CN triple bonds, confirming its synthesis. As displayed in Fig. 1(c), the spectra of the Pyrene-CTFs featured absorption bands at 1565 and 1365 cm^{-1} representing the triazine rings, but

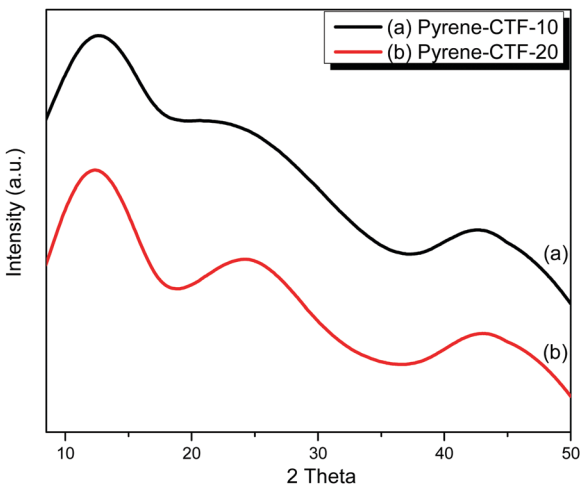

Fig. 4 XRD patterns of Pyrene-CTF-10 and Pyrene-CTF-20.

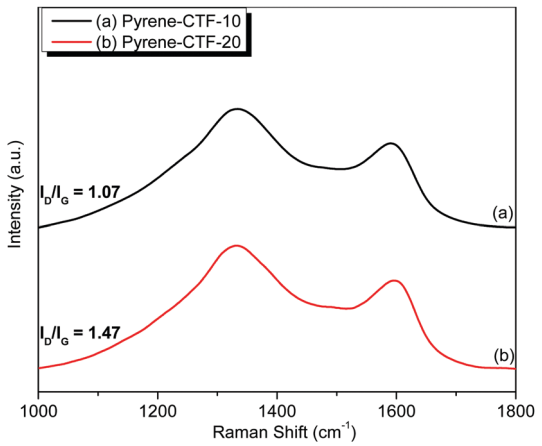

Fig. 5 Raman spectra of Pyrene-CTF-10, and Pyrene-CTF-20.

no signals for CN groups, confirming the successful trimerization/cyclization reactions of the cyano groups.[8,28,60] In addition, the intensities of the characteristics absorption bands of the triazine ring in Pyrene-CTF-20 gradually decreased at 500 °C, due to the occurrence partial carbonization [Fig. S1, ESI†].[61,62] We performed FTIR spectral analyses to monitor the trimerization of the nitrile groups in the preparation of Pyrene-CTF-10 from room temperature to 500 °C (Fig. 2). For temperatures between 25 and 300 °C, the FTIR spectrum of Pyrene-CTF-10 featured the characteristic absorption band at 2220 cm^{-1} for stretching of the CN triple bonds. When the temperature reached 500 °C, however, this characteristic band disappeared completely and two new absorption signals appeared at 1565 and 1360 cm^{-1}, confirming the complete trimerization of the nitrile groups and the formation of triazine rings.[28]

We used solid state ^{13}C CP/MAS NMR spectroscopy (Fig. S2, ESI†) to confirm the chemical structures of TBrPy and TCNPy and the formation of triazine rings in the Pyrene-CTFs materials. The solid state ^{13}C NMR spectrum of TBrPy [Fig. S2(a), ESI†] displays signals at 127, 116 and 110 ppm at for the aromatic carbon atoms. Fig. S2(b) (ESI†) reveals that the spectrum of TCNPy features signals at 132 and 108 ppm for the aromatic carbon nuclei and signal at 116 ppm for CN group. The solid state ^{13}C NMR spectra [Fig. S2(c and d), ESI†] of Pyrene-CTF-10 and Pyrene-CTF-20 exhibited signals at 168, 136, 123 and 116 ppm which we assign to the carbon nuclei of the triazine [–C(Ar)═N–] and the pyrene units.[8,28,63] We determined the thermal stabilities of TCNPy, Pyrene-CTF-10, and Pyrene-CTF-20 through TGA under a N_2 atmosphere (Fig. 3). Although Pyrene-CTF-10 and Pyrene-CTF-20 were synthesized in molten $ZnCl_2$ at 500 °C, the decomposition temperature (T_{d10}) of Pyrene-CTF-10 (500 °C) was higher than that of Pyrene-CTF-20 (474 °C); they had the same char yield of 71 wt%. These values for the TCNPy monomer were 346 °C and 4 wt%, respectively. Thus, these Pyrene-CTFs displayed outstanding thermal stability.[8,28]

Fig. 4 provides the XRD patterns of Pyrene-CTF-10 and Pyrene-CTF-20, revealing that they had partially crystalline structures with two broad peaks at 13° and 25° that we assign to the vertical spacing between stacked sheets (001) and the in-plane reflection (100), respectively.[15,64] Fig. 5 presents the Raman spectra of Pyrene-CTF-10 and Pyrene-CTF-20 in the range from 1000 to 1900 cm^{-1}. The spectra of both Pyrene-CTFs materials featured two strong signals characteristic of D and G bands, suggesting the existence of graphitic carbonized structures. In general, the D and G bands represent the graphitic carbon atoms: second-order Raman scattering with sp^3 hybridization and first-order Raman scattering with sp^2 hybridization, respectively.[15,28,64,65] From the Raman spectra of Pyrene-CTF-10 and Pyrene-CTF-20, the D bands were centered at 1342 and 1335 cm^{-1}, respectively, while the G bands appeared at 1584 and 1586 cm^{-1}, respectively. The I_D/I_G ratios for Pyrene-CTF-10 and Pyrene-CTF-20 were 1.07 and 1.47, respectively.

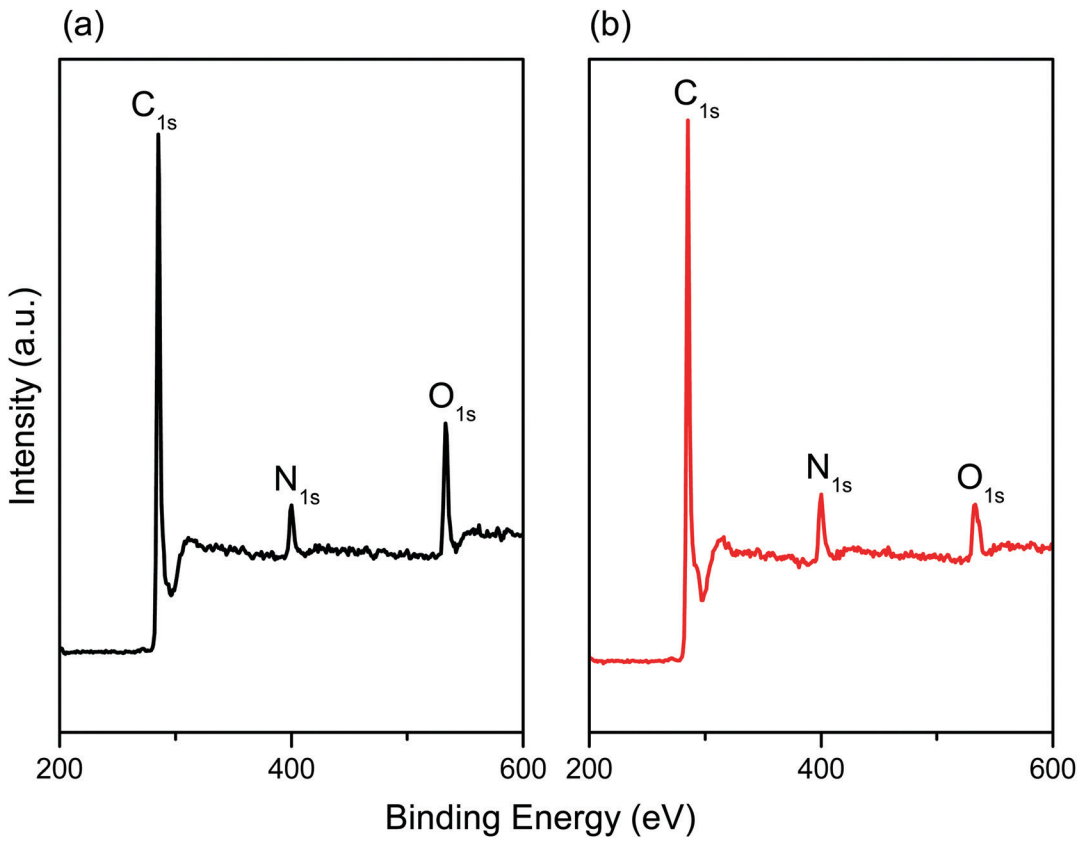

Fig. 6 XPS survey spectra of (a) Pyrene-CTF-10 and (b) Pyrene-CTF-20.

Thus, Pyrene-CTF-10 possessed a lower degree of graphitization and featured less defects in its structure when compared with Pyrene-CTF-20.

Fig. 6 displays the XPS spectra of the Pyrene-CTFs. Three peaks appeared in each spectrum: at 284 eV (for carbon atoms in the polymeric CTF framework), 400 eV (C–N bonds for the N 1s orbitals in the triazine units), and 530 eV (O 1s orbitals for absorbed water and oxygen), respectively.[28,53,66,67]

We fitted the XPS curves for the N 1s and O 1s orbitals to investigate the chemical compositions on the surfaces of these Pyrene-CTFs (Fig. 7 and Table 2). The fitting results for the N 1s orbitals [Fig. 7(a and b)] revealed the presence of three N species, including quaternary-N species (401 eV), pyrrolic species (400 eV), and hexagonal pyridinic N atoms from the triazine ring (398.7 eV). According to quantitative analysis, the pyrrolic N and pyridinic species were the most abundant in the Pyrene-CTF frameworks. Furthermore, the surfaces of the Pyrene-CTF materials contained three O species [Fig. 7(c and d)], with signals at 531, 532, and 533 eV corresponding to polarized C–O bonds, water, and absorbed oxygen.[28,53,66,67]

We measured N_2 adsorption/desorption isotherms (Fig. 8 and Table 1) at 77 K to examine the porosities of our Pyrene-CTFs. Fig. 8(a) reveals that Pyrene-CTF-10 had microporous characteristics, with a specific surface area of 819 $m^2\ g^{-1}$ and a pore volume of 0.88 $cm^3\ g^{-1}$. The BET curve of Pyrene-CTF-20 featured a type IV isotherm, with a high specific surface area of 1019 $m^2\ g^{-1}$ and a pore volume of 1.12 $cm^3\ g^{-1}$. Thus, the specific BET surface area of Pyrene-CTF-20 was higher than that of Pyrene-CTF-10, suggesting the presence of closely packed nanoparticles and a larger number of defects in the Pyrene-CTF-20 structure.[8,28] Furthermore, we used NL-DFT theory to calculate the pore diameters in Pyrene-CTF-10 and Pyrene-CTF-20 [Fig. 8(b) and Table 1] to be 1.10 and 1.35 nm, respectively. TEM images (Fig. 9) revealed that Pyrene-CTF-10 and Pyrene-CTF-20 both possessed irregular microporous structures.

Table 2 Curve-fitting data and area fractions of the signals in the N 1s and O 1s plots in Fig. 7

	N species			O species		
Sample	N-6	N-5	N-Q	C–O	C–OH	H_2O
Pyrene-CTF-10	68.24	21.44	10.32	45.29	15.61	39.10
Pyrene-CTF-20	59.92	23.97	16.12	69.16	15.58	30.84

Energy storage and CO_2 uptake of Pyrene-CTFs

From the BET and XPS data, we knew that our Pyrene-CTF materials had high specific surface areas, N-heteroatom frameworks (primarily pyridinic and pyrrolic N species), and mesoporous and microporous properties. Therefore, we expected these materials to have great potential applications in energy storage and gas uptake.[21] We measured the electrochemical properties of the Pyrene-CTFs through cyclic voltammetry (CV)

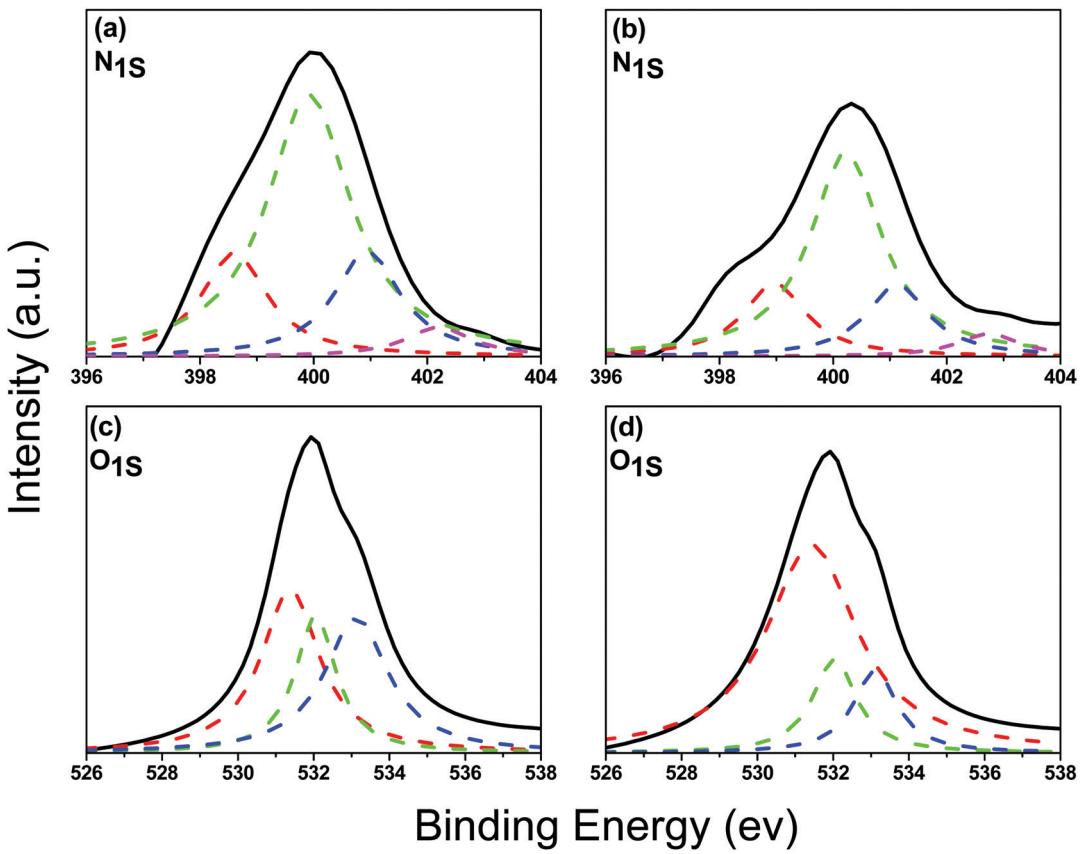

Fig. 7 XPS fitting curves of N 1s and O 1s orbitals: (a and c) Pyrene-CTF-10; (b and d) Pyrene-CTF-20.

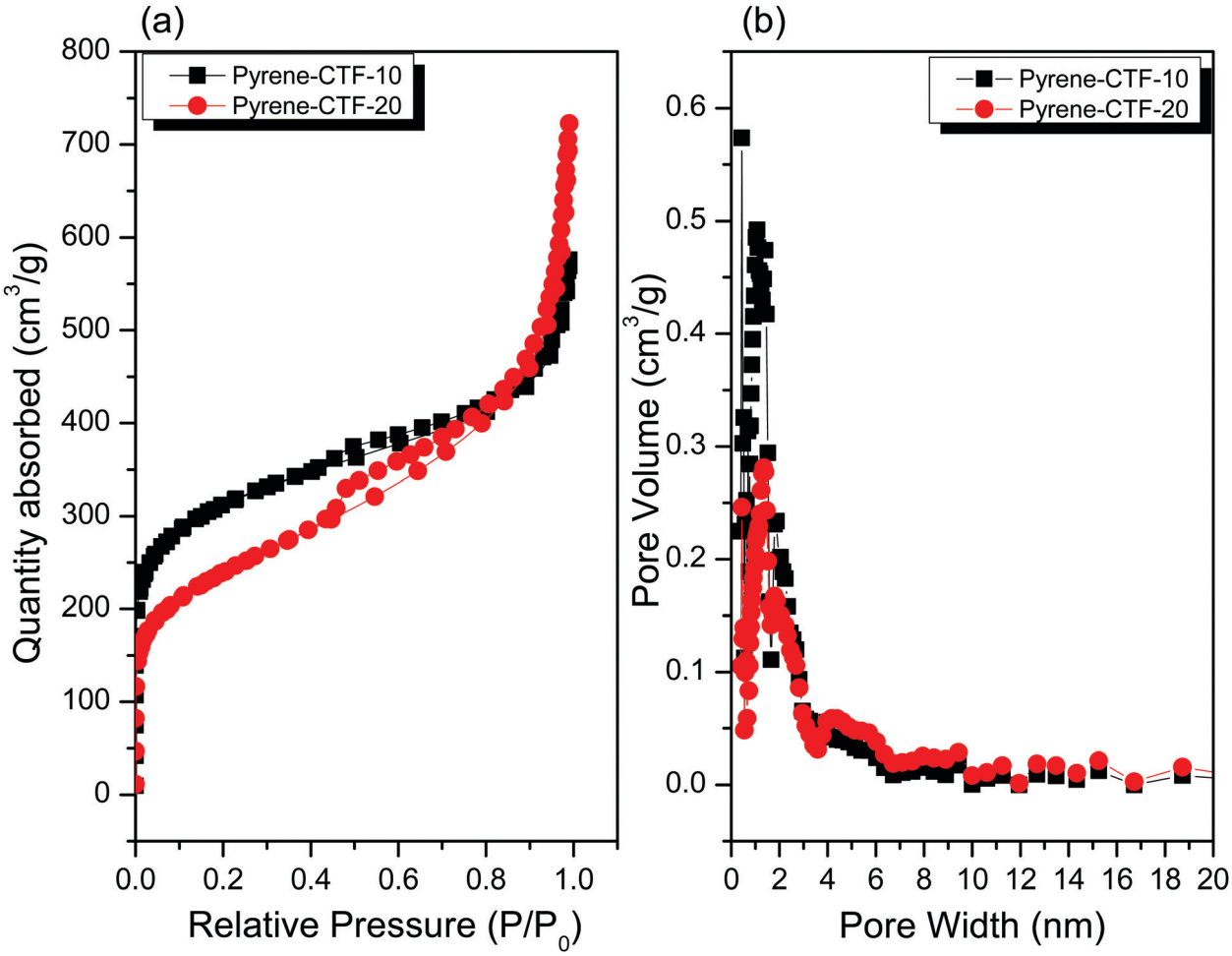

Fig. 8 (a) N_2 adsorption/desorption measurements and (b) pore size distributions of Pyrene-CTF-10 and Pyrene-CTF-20, recorded at 77 K.

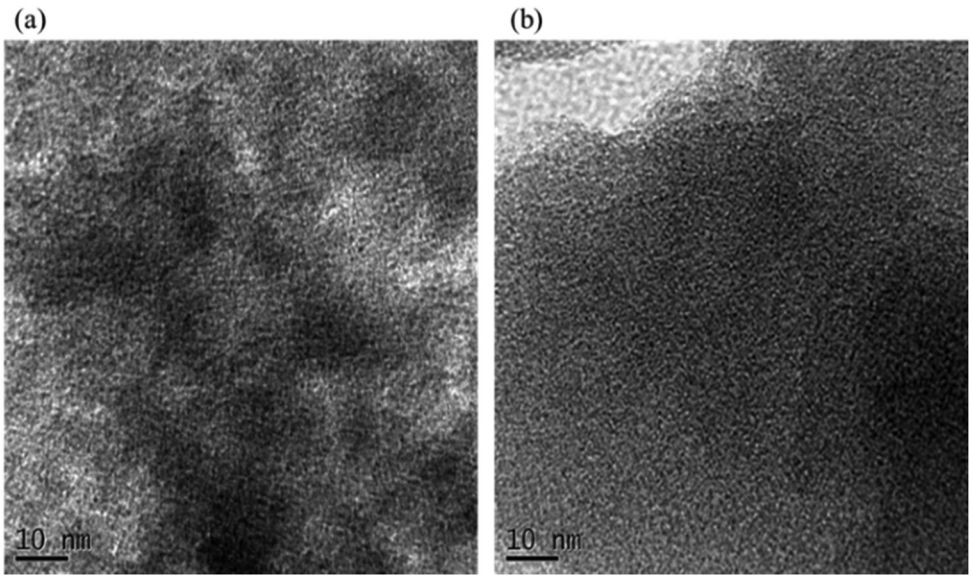

Fig. 9 TEM images of (a) Pyrene-CTF-10 and (b) Pyrene-CTF-20.

at various scan rates (5–200 mV s^{-1}) in 1 M aqueous KOH [Fig. 10(a and b)]. The CV profiles for the Pyrene-CTFs had rectangular (''rice-like'') shapes.[2,4,28] The appearance of rectangular CV curves for these CTF materials based on pyrene units

suggested a combination of electric double-layer capacitance and pseudocapacitance, arising from the presence of various types of nitrogen and oxygen species (heteroatom effects, based on XPS data) in both of these polymeric CTF materials.[2,4,28] In addition, the galvanostatic charge/discharge (GCD) profiles of Pyrene-CTF-10 and Pyrene-CTF-20 recorded at various current densities [Fig. 10(c and d)] had triangular shapes, again suggesting the presence of both EDLC and pseudocapacitance arising from the graphitic carbon structures presenting various types of functionalized units (*e.g.*, pyrrolic species; hexagonal pyridinic N atoms in triazine rings; C=O and phenolic OH groups).[2,21] As displayed in Fig. 10(e), at a current density of 0.5 A g^{-1}, Pyrene-CTF-10 and Pyrene-CTF-20 displayed excellent specific capacitances of 380 and 500 F g^{-1}, respectively. The higher specific capacitance of pyrene-CTF-20 compared with that of Pyrene-CTF-10 presumably arose from its graphitic structure, microporosity, and high N (7.19 wt%) and O atom (9.62 wt%) contents. In addition, the specific capacitances of the Pyrene-CTFs decreased upon increasing the scan rate, due to the adsorption of electrolyte ions on the electrode surfaces.[8,68,69] In addition, we investigated the cyclic stabilities of Pyrene-CTF-10 and Pyrene-CTF-20 through GCD measurements over 2000 cycles at a current density of 10 A g^{-1} [Fig. 10(f)]. Pyrene-CTF-10 and Pyrene-CTF-20 both retained 97% of their initial capacitance after 2000 cycles, indicating their excellent cycling stability in 1 M KOH as the electrolyte. Deng *et al.* prepared conductive CTFs through ionothermal reactions of tetracyanoquinodimethane (TCNQ) in the presence of molten $ZnCl_2$ at various temperatures. They found that the specific capacitances of TCNQ-CTF-600, TCNQ-CTF-700, TCNQ-CTF-800, and TCNQ-CTF-900 at a current density of 0.2 A g^{-1} were 284, 350, 380, and 356 F g^{-1}, respectively. The highest specific capacitance (380 F g^{-1}) was that of TCNQ-CTF-800, presumably because of its high N-atom content (8.13%) and large surface area (3663 m^2 g^{-1}).[2] In addition, Zhi *et al.* derived amorphous CTFs from terephthalonitrile that displayed a

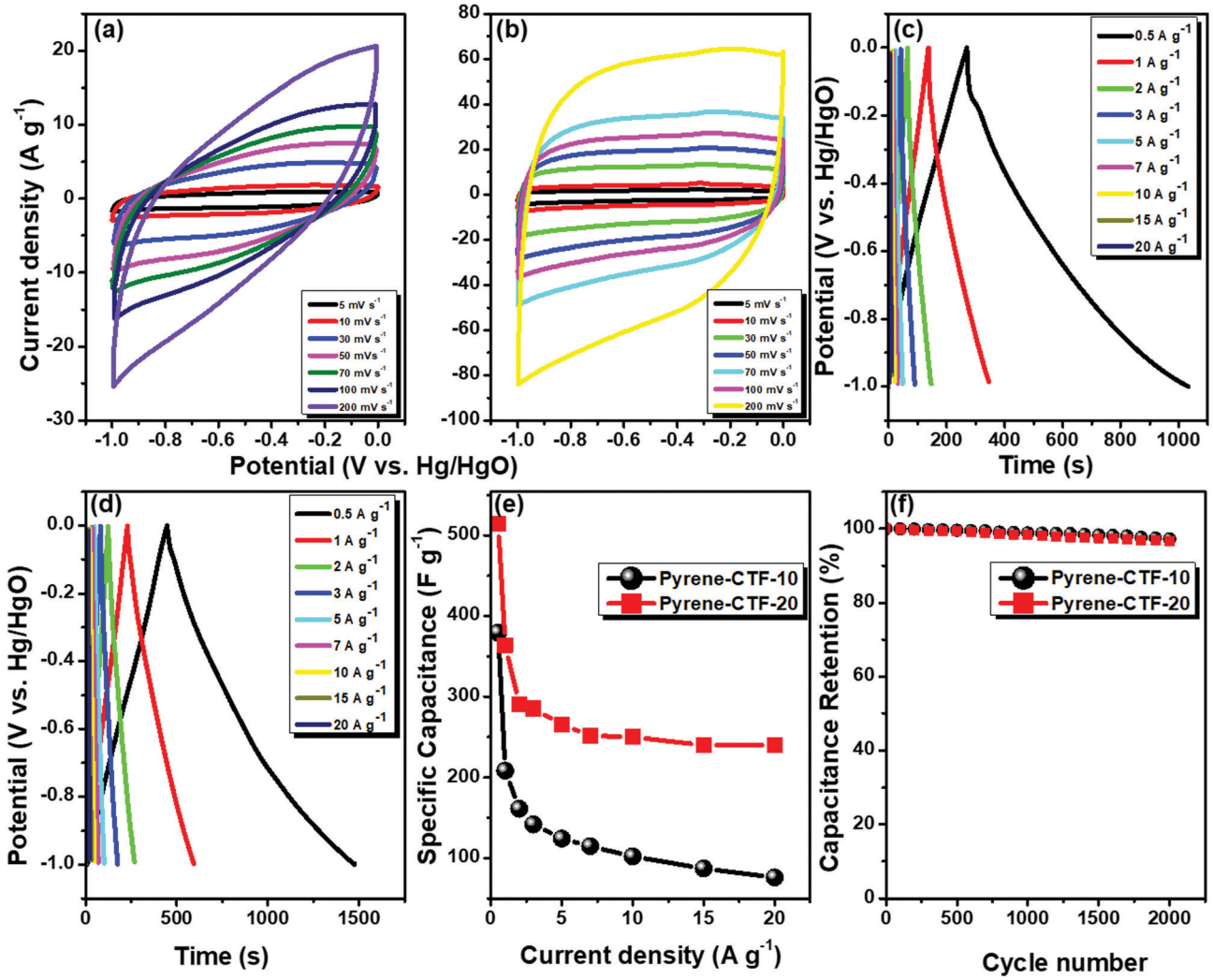

Fig. 10 (a and b) CV curves of Pyrene-CTF-10 and Pyrene-CTF-20. (c and d) GCD profiles of Pyrene-CTF-10 and Pyrene-CTF-20, recorded at various currents. (e) Specific capacitances of Pyrene-CTF-10 and Pyrene-CTF-20 recorded at current densities from 0.5 to 20 A g^{-1}. (f) Cycling stabilities of Pyrene-CTF-10 and Pyrene-CTF-20 electrodes, recorded at a current density of 10 A g^{-1} over 2000 cycles.

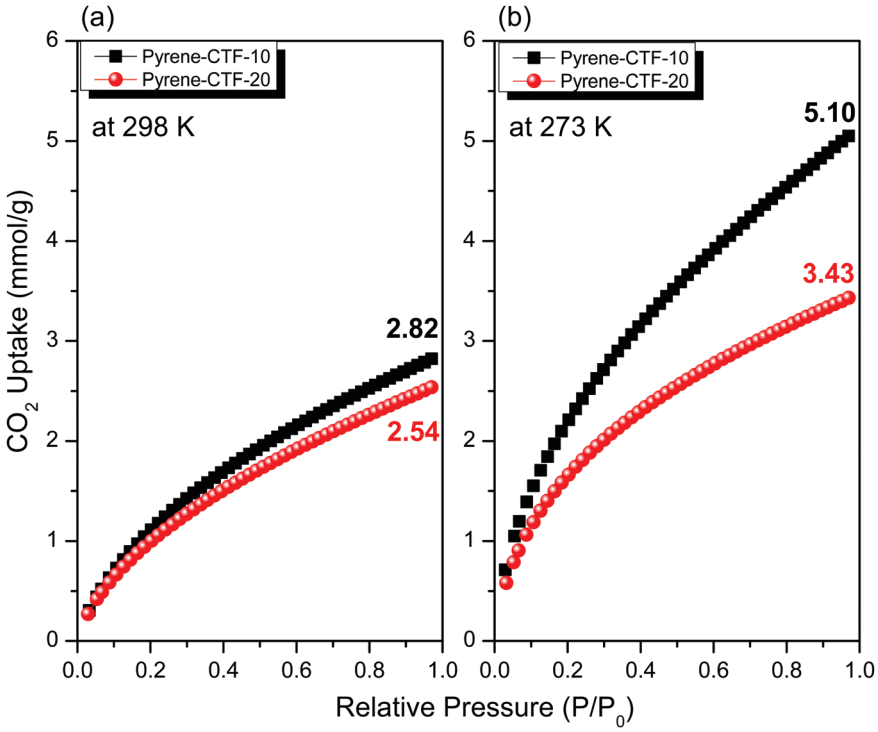

Fig. 11 CO_2 uptake of (a) Pyrene-CTF-10 and (b) Pyrene-CTF-20, measured at 298 and 273 K.

specific capacitance of 298 F g^{-1} at 0.2 A g^{-1}.[70] In addition, we have previously reported a series of Car-CTFs formed through trimerization of Car-4CN with molten $ZnCl_2$; among them, Car-CFT-5-500 provided a specific capacitance of 545 F g^{-1} at 5 mV s^{-1}.[28] In comparison with these other CTF materials, Pyrene-CTF-20 displays excellent supercapacitor performance (Table S1, ESI†), presumably because of its graphitic structure, microporosity, and N and O atom contents. Fig. S3 (ESI†) shows that the calculated coulombic efficiency (CE) with the current density. It shows that the CE is very high at current density of 0.5 and 1 A g^{-1}, this is due to the very small applied charging and discharging currents. While at current density >1 A g^{-1}, the CE is almost ~100%. We recorded CO_2 adsorption isotherms for both Pyrene-CTFs at 25 and 0 °C [Fig. 11(a and b)]. The CO_2 uptake of Pyrene-CTF-10 was 2.82 and 5.10 mmol g^{-1} at 25 and 0 °C, respectively; for Pyrene-CTF-20, these values were lower at 2.54 and 3.43 mmol g^{-1}, respectively. Thus, Pyrene-CTF-10 captured more CO_2 at 25 °C (2.82 mmol g^{-1}) than other previously reported CTF materials at the same temperature, including Car-CTF-10-500 (2.25 mmol g^{-1}),[28] CTF-1 (2.77 mmol g^{-1}),[71] PCTF-1-3 (2.02–3.00 mmol g^{-1}),[72] CTF-20-400 (3.48 mmol g^{-1}),[3] CTF-0 (1.54–2.34 mmol g^{-1}),[73] and CTF-DCN-500 (2.70 mmol g^{-1}),[62] due to Pyrene-CTF-10 having a specific surface area of 819 m^2 g^{-1} and a high N-atom content (9.85 wt%) arose from the presences of triazine units, which leads to increase the binding affinity interaction between CO_2 molecules and Pyrene-CTF-10. Table S2 (ESI†) provides a performance comparison Pyrene-CTFs and other reported CTFS for CO_2 uptake. Thus, our CV and CO_2 uptake measurements suggest that Pyrene-CTFs have great potential for use in energy storage and gas storage.

Conclusions

We have synthesized two pyrene-containing conductive CTFs, Pyrene-CTF-10 and Pyrene-CTF-20, through reactions of TCNPy with molten $ZnCl_2$ (as catalyst) at 500 °C. These Pyrene-CTFs exhibited outstanding thermal stabilities (high char yields), partial crystallinity, and high specific surface areas, based on BET, XRD, and TGA analyses. In addition, Pyrene-CTF-10 displayed gas uptake capacities for CO_2 of 2.82 mmol g^{-1} at 25 °C and 5.10 mmol g^{-1} at 0 °C. More interestingly, the electrochemical performances of our two Pyrene-CTFs were highly stable and efficient, with highest capacitances at 0.5 mV s^{-1} of 380 F g^{-1} for Pyrene-CTF-10 and 500 F g^{-1} for Pyrene-CTF-20.

Characterization

FTIR spectra were recorded using a Bruker Tensor 27 FTIR spectrophotometer and the conventional KBr disk method; 32 scans were collected at a spectral resolution of 4 cm^{-1}. The films used in this study were sufficiently thin to obey the Beer–Lambert law. Wide-angle X-ray diffraction (WAXD) pattern was obscured from the wiggler beamline BL17A1 of the National Synchrotron Radiation Research Center (NSRRC), Taiwan. A triangular bent Si(111) single crystal was used to obtain a monochromated beam having a wavelength (λ) of 1.33 Å. Cross-polarization with MAS (CPMAS) was used to acquire ^{13}C NMR spectral data at 75.5 MHz. The CP contact time was 2 ms; ^{1}H decoupling was applied during data acquisition. The decoupling frequency corresponded to 32 kHz. The MAS sample spinning rate was 10 kHz. Transmission electron microscope (TEM) images were obtained with a JEOL JEM-2010

instrument operated at 200 kV. BET surface area and porosimetry measurements of the prepared samples (*ca.* 40–100 mg) were performed using a Micromeritics ASAP 2020 Surface Area and Porosity analyzer. Nitrogen isotherms were generated through incremental exposure to ultrahigh-purity N_2 (up to *ca.* 1 atm) in a liquid nitrogen (77 K) bath. Surface parameters were determined using BET adsorption models in the instrument's software. TGA was performed using a TA Q-50 analyzer under a flow of N_2 atmosphere. The samples were sealed in a Pt cell and heated from 40 to 800 °C at a heating rate of 20 °C min^{-1} under a flow of N_2 atmosphere at a flow rate of 60 mL min^{-1}. The Raman spectra were investigated using Horiba Jobin-Yvon HR800 Raman Spectrometer with 633 nm laser, 10 s accumulated scans repeated for 20 times and 50× magnification lens. The electrochemical performances were performed using Zahner Zennium E electrochemical workstation with three electrodes configurations using Hg/HgO as a reference electrode and 1.0 M KOH solution as an aqueous medium. The working electrode was the glassy carbon electrode (GCE) coated by the slurry of the tested material (the slurries were prepared by dispersing the Pyrene-CTFs (45 wt%), carbon black (45 wt%), and Nafion (10 wt%) in EtOH (1 mL)). The cyclic voltammetry (CV) was tested over the range between 0.0 and −1.0 V and the scan rates were investigated from 5 mV s^{-1} up to 200 mV s^{-1}. Similarly, the charge and discharge (GCD) cycles were tested at the same potential range with different current densities from 0.5 to 20 A g^{-1}. The capacitances (C_s) were calculated using the reported equations for CV and GCD respectively.[74,75]

Conflicts of interest

There are no conflicts to declare.

Acknowledgements

This study was supported financially by the Ministry of Science and Technology, Taiwan, under contracts under contracts MOST 106-2221-E-110-067-MY3, 108-2638-E-002-003-MY2, and 108-2221-E-110-014-MY3. We also thank Mr Hsien-Tsan Lin of the Regional Instruments Center at National Sun Yat-Sen University for help with the TEM measurement.

Notes and references

1 P. Bhanja, S. K. Das, K. Bhunia, D. Pradhan, T. Hayashi, Y. Hijikata, S. Irle and A. Bhaumik, A New Porous Polymer for Highly Efficient Capacitive Energy Storage, *ACS Sustainable Chem. Eng.*, 2018, **6**, 202–209.

2 Y. Li, S. Zheng, X. Liu, P. Li, L. Sun, R. Yang, S. Wang, Z. Wu, X. Bao and W. Q. Deng, Conductive Microporous Covalent Triazine-Based Framework for High-Performance Electrochemical Capacitive Energy Storage, *Angew. Chem., Int. Ed.*, 2018, **57**, 7992–7996.

3 P. Simon and Y. Gogotsi, Materials for electrochemical capacitors, *Nat. Mater.*, 2008, **7**, 845–854.

4 Y. Liu, X. Hao, L. Wang, Y. Xu, J. Liu, X. Tian and B. Yao, Facile synthesis of porous carbon materials with extra high nitrogen content for supercapacitor electrodes, *New J. Chem.*, 2019, **43**, 3713–3718.

5 Z. S. Wu, K. Parvez, X. Feng and K. Muellen, Graphene-based in-plane micro-supercapacitors with high power and energy densities, *Nat. Commun.*, 2013, **4**, 2487.

6 D. M. D'Alessandro, B. Smit and J. R. Long, Carbon Dioxide Capture: Prospects for New Materials, *Angew. Chem., Int. Ed.*, 2010, **49**, 6082.

7 Q. Wang, J. Luo, Z. Zhong and A. Borgna, CO_2 capture by solid adsorbents and their applications: current status and new trends, *Energy Environ. Sci.*, 2011, **4**, 42–55.

8 G. Wang, K. Leus, S. Zhao and P. V. D. Voort, Newly Designed Covalent Triazine Framework Based on Novel N-Heteroaromatic Building Blocks for Efficient CO_2 and H_2 Capture and Storage, *ACS Appl. Mater. Interfaces*, 2018, **10**, 1244–1249.

9 S. P. Lee, N. Mellon, A. M. Sharif and J. M. Leveque, Geometry variation in porous covalent triazine polymer (CTP) for CO_2 adsorption, *New J. Chem.*, 2018, **42**, 15488–15496.

10 G. T. Rochelle, Amine Scrubbing for CO_2 Capture, *Science*, 2009, **325**, 1652–1654.

11 A. B. Rao and E. S. Rubin, A Technical, Economic, and Environmental Assessment of Amine-Based CO_2 Capture Technology for Power Plant Greenhouse Gas Control, *Environ. Sci. Technol.*, 2002, **36**, 4467–4475.

12 F. M. Orr Jr, CO_2 capture and storage: are we ready?, *Energy Environ. Sci.*, 2009, **2**, 449–458.

13 R. S. Haszeldine, Carbon capture and storage: how green can black be?, *Science*, 2009, **325**, 1647–1652.

14 D. M. D'Alessandro, B. Smit and J. R. Long, Carbon dioxide capture: prospects for new materials, *Angew. Chem., Int. Ed.*, 2010, **49**, 6058–6082.

15 S. Mukherjee, M. Das, A. Manna, R. Krishna and S. Das, Dual Strategic Approach to Prepare Defluorinated Triazole-Embedded Covalent Triazine Frameworks with High Gas Uptake Performance, *Chem. Mater.*, 2019, **31**, 3929–3940.

16 Y. Xu, S. Jin, H. Xu, A. Nagai and D. Jiang, Conjugated microporous polymers: design, synthesis and application, *Chem. Soc. Rev.*, 2013, **42**, 8012.

17 S. Wang, Y. Liu, Y. Ye, X. Meng, J. Du, X. Song and Z. Liang, Ultrahigh volatile iodine capture by conjugated microporous polymer based on N,N,N',N'-tetraphenyl-1,4-phenylenediamine, *Polym. Chem.*, 2019, **10**, 2608–2615.

18 Q. Sun, Z. F. Dai, X. J. Meng and F. S. Xiao, Porous polymer catalysts with hierarchical structures, *Chem. Soc. Rev.*, 2015, **44**, 6018–6034.

19 Y. Xu, N. Mao, C. Zhang, X. Wang, J. Zeng, Y. Chen, F. Wang and J. X. Jiang, Rational design of donor-π-acceptor conjugated microporous polymers for photocatalytic hydrogen production, *Appl. Catal., B*, 2018, **228**, 1–9.

20 W. K. Meng, L. Liu, X. Wang, R. S. Zhao, M. L. Wang and J. M. Lin, Polyphenylene core-conjugated microporous

polymer coating for highly sensitive solid-phase microextraction of polar phenol compounds in water samples, *Anal. Chim. Acta*, 2018, **1015**, 27–34.

21 S. Dutta, A. Bhaumik and K. C. W. Wu, hierarchically porous carbon derived from polymers and biomass: effect of interconnected pores on energy applications, *Energy Environ. Sci.*, 2014, **7**, 3574–3592.

22 S. Xu, J. He, S. Jin and B. Tan, Heteroatom-rich porous organic polymers constructed by benzoxazine linkage with high carbon dioxide adsorption affinity, *J. Colloid Interface Sci.*, 2018, **509**, 457–462.

23 A. F. M. EL-Mahdy, T. E. Liu and S. W. Kuo, Direct Synthesis of Nitrogen-Doped Mesoporous Carbons from Triazine-Functionalized Resol for CO_2 Uptake and Highly Efficient Removal of Dyes, *J. Hazard. Mater.*, 2020, **391**, 122163.

24 A. F. M. EL-Mahdy, Y. H. Hung, T. H. Mansoure, H. H. Yu, Y. S. Hsu, K. C. W. Wu and S. W. Kuo, Synthesis of [3+ 3] β-ketoenamine-tethered covalent organic frameworks (COFs) for high-performance supercapacitance and CO_2 storage., *J. Taiwan Inst. Chem. Eng.*, 2019, **103**, 199–208.

25 Y. Zhao, N. Bu, H. Shao, Q. Zhang, B. Feng, Y. Xu, G. Zheng, Y. Yuan, Z. Yan and L. Xi, A carbonized porous aromatic framework to achieve customized nitrogen atoms for enhanced supercapacitor performance, *New J. Chem.*, 2019, **43**, 18158–18164.

26 H. Wang, Z. Cheng, Y. Liao, J. Li, J. Weber, A. Thomas and C. F. J. Faul, Conjugated Microporous Polycarbazole Networks as Precursors for Nitrogen-Enriched Microporous Carbons for CO_2 Storage and Electrochemical Capacitors, *Chem. Mater.*, 2017, **29**, 4885–4893.

27 (*a*) A. F. M. EL-Mahdy, M. G. Mohamed, T. H. Mansoure, H. H. Yu, T. Chen and S. W. Kuo, Ultrastable tetraphenyl-p-phenylenediamine-based covalent organic frameworks as platforms for high-performance electrochemical supercapacitors, *Chem. Commun.*, 2019, **55**, 14890–14893; (*b*) X. Li, X. Yang, H. Xue, H. Xue, H. Pang and Q. Xu, Metal–organic frameworks as a platform for clean energy applications, *EnergyChem*, 2020, **2**, 100027.

28 M. G. Mohamed, A. F. M. EL-Mahdy, M. M. M. Ahmed and S. W. Kuo, Direct Synthesis of Microporous Bicarbazole-Based Covalent Triazine Frameworks for High-Performance Energy Storage and Carbon Dioxide Uptake, *ChemPlusChem*, 2019, **84**, 1767–1774.

29 M. G. Rabbani, A. K. Sekizkardes, O. M. El-Kadri, B. R. Kaafarani and H. M. El-Kaderi, Pyrene-directed growth of nanoporous benzimidazole-linked nanofibers and their application to selective CO_2 capture and separation, *J. Mater. Chem.*, 2012, **22**, 25409–25417.

30 Q. Chen, M. Luo, P. Hammershøj, D. Zhou, Y. Han, B. W. Laursen, C. G. Yan and B. H. Han, Microporous Polycarbazole with High Specific Surface Area for Gas Storage and Separation, *J. Am. Chem. Soc.*, 2012, **134**, 6084–6087.

31 N. Popp, T. Homburg, N. Stock and J. Senker, Porous imine-based networks with protonated imine linkages for carbon dioxide separation from mixtures with nitrogen and methane, *J. Mater. Chem. A*, 2015, **3**, 18492–18504.

32 (*a*) A. F. M. EL-Mahdy, C. Young, J. Kim, J. You, Y. Yamauchi and S. W. Kuo, Hollow Microspherical and Microtubular [3 + 3] Carbazole-Based Covalent Organic Frameworks and Their Gas and Energy Storage Applications, *ACS Appl. Mater. Interfaces*, 2019, **11**, 9343–9354; (*b*) Z. Liang, R. Zhao, T. Qiu, R. Zou and Q. Xu, Metal-organic framework- derived materials for electrochemical energy applications, *EnergyChem*, 2019, **1**, 100001.

33 (*a*) A. F. M. EL-Mahdy, C. H. Kuo, A. Alshehri, C. Young, Y. Yamauchi, J. Kim and S. W. Kuo, Strategic design of triphenylamine-and triphenyltriazine-based two-dimensional covalent organic frameworks for CO_2 uptake and energy storage, *J. Mater. Chem. A*, 2018, **6**, 19532–19541; (*b*) X. C. Li, Y. Zhang, C. Y. Wang, Y. Wan, W. Y. Lai, H. Pang and W. Huang, Redox-active triazatruxene-based conjugated microporous polymers for high-performance supercapacitors, *Chem. Sci.*, 2017, **8**, 2959–2965.

34 C. Li, P. Li, L. Chen, M. E. Briggs, M. Liu, K. Chen, X. Shi, D. Han and S. Ren, Pyrene-Cored Covalent Organic Polymers by Thiophene-Based Isomers, Their Gas Adsorption, and Photophysical Properties, *J. Polym. Sci., Part A: Polym. Chem.*, 2017, **55**, 2383–2389.

35 Z. Xiang and D. Cao, Porous covalent–organic materials: synthesis, clean energy application and design, *J. Mater. Chem. A*, 2013, **1**, 2691–2718.

36 A. K. Sekizkardes, T. İslamoğlu, Z. Kahveci and H. M. El-Kaderi, Application of pyrene-derived benzimidazole-linked polymers to CO_2 separation under pressure and vacuum swing adsorption settings, *J. Mater. Chem. A*, 2014, **2**, 12492–12500.

37 A. Bhunia, V. Vasylyeva and C. Janiak, From a supramolecular tetranitrile to a porous covalent triazine-based framework with high gas uptake capacities, *Chem. Commun.*, 2013, **49**, 3961–3963.

38 H. R. Abuzeid, A. F. M. EL-Mahdy, M. M. M. Ahmed and S. W. Kuo, Triazine-functionalized covalent benzoxazine framework for direct synthesis of N-doped microporous carbon, *Polym. Chem.*, 2019, **10**, 6010–6020.

39 P. Kuhn, A. Forget, J. Hartmann, A. Thomas and M. Antonietti, Template-Free Tuning of Nanopores in Carbonaceous Polymers through Ionothermal Synthesis, *Adv. Mater.*, 2009, **21**, 897.

40 P. Kuhn, M. Antonietti and A. Thomas, Porous, Covalent Triazine-Based Frameworks Prepared by Ionothermal Synthesis, *Angew. Chem., Int. Ed.*, 2008, **47**, 3450.

41 T. Xu, Y. Li, Z. Zhao, G. Xing and L. Chen, N,N'-Bicarbazole-Based Covalent Triazine Frameworks as High-Performance Heterogeneous Photocatalysts, *Macromolecules*, 2019, **52**, 9786–9791.

42 J. Guo, L. Wang and J. Huang, Porphyrin-Based Triazine Polymers and Their Derived Porous Carbons for Efficient CO_2 Capture, *Ind. Eng. Chem. Res.*, 2020, **59**(7), 3205–3212.

43 A. F. M. El-Mahdy, Y. H. Hung, T. H. Mansoure, H. H. Yu, T. Chen and S. W. Kuo, A Hollow Microtubular Triazine- and Benzobisoxazole-Based Covalent Organic Framework Presenting Sponge-Like Shells That Functions as a

High-Performance Supercapacitor, *Chem. – Asian J.*, 2019, **14**, 1429–1435.

44 W. Yu, S. Gu, Y. Fu, S. Xiong, C. Pan, Y. Liu and G. Yu, Carbazole-decorated covalent triazine frameworks: Novel nonmetal catalysts for carbon dioxide fixation and oxygen reduction reaction, *J. Catal.*, 2018, **362**, 1–9.

45 L. Guo, Y. Niu, H. Xu, Q. Li, S. Razzaque, Q. Huang, S. Jin and B. Tan, Engineering heteroatoms with atomic precision in donor–acceptor covalent triazine frameworks to boost photocatalytic hydrogen production, *J. Mater. Chem. A*, 2018, **6**, 19775–19781.

46 (*a*) F. Xu, S. Yang, G. Jiang, Q. Ye, B. Wei and H. Wang, Fluorinated, Sulfur-Rich, Covalent Triazine Frameworks for Enhanced Confinement of Polysulfides in Lithium–Sulfur Batteries, *ACS Appl. Mater. Interfaces*, 2017, **9**, 37731–37738; (*b*) G. Liu, Y. Sheng, J. W. Ager, M. Kraft and R. Xu, Research advances towards large-scale solar hydrogen production from water, *EnergyChem*, 2019, **1**, 100014.

47 J. Liu, P. Lyu, Y. Zhang, P. Nachtigall and Y. Xu, New Layered Triazine Framework/Exfoliated 2D Polymer with Superior Sodium-Storage Properties, *Adv. Mater.*, 2018, **30**, 1705401.

48 M. Liu, L. Guo, S. Jin and B. Tan, Covalent triazine frameworks: synthesis and applications, *J. Mater. Chem. A*, 2019, **7**, 5153–5172.

49 S. Dalapati, S. Jin, J. Gao, Y. Xu, A. Nagai and D. Jiang, An Azine-Linked Covalent Organic Framework, *J. Am. Chem. Soc.*, 2013, **135**, 17310–17313.

50 G. Lin, H. Ding, D. Yuan, B. Wang and C. Wang, A Pyrene-Based, Fluorescent Three-Dimensional Covalent Organic Framework, *J. Am. Chem. Soc.*, 2016, **138**, 3302–3305.

51 R. S. Sprick, J. X. Jiang, B. Bonillo, S. Ren, T. Ratvijitvech, P. Guiglion, M. A. Zwijnenburg, D. J. Adams and A. I. Cooper, *J. Am. Chem. Soc.*, 2015, **137**, 3265–3270.

52 A. Bhunia, V. Vasylyeva and C. Janiak, From a supramolecular tetranitrile to a porous covalent triazine-based framework with high gas uptake capacities, *Chem. Commun.*, 2013, **49**, 3961–3963.

53 X. M. Hu, Q. Chen, Y. C. Zhao, B. W. Laursen and B. H. Han, Straightforward synthesis of a triazine-based porous carbon with high gas-uptake capacities, *J. Mater. Chem. A*, 2014, **2**, 14201–14208.

54 P. J. Waller, Y. S. AlFaraj, C. S. Diercks, N. N. Jarenwattananon and O. M. Yaghi, Conversion of Imine to Oxazole and Thiazole Linkages in Covalent Organic Frameworks, *J. Am. Chem. Soc.*, 2018, **140**, 9099–9103.

55 X. Yin, Y. Peng, J. Luo, X. Zhou, C. Gao, L. Wang and C. Yang, Tailoring the framework of organic small molecule semiconductors towards high-performance thermoelectric composites via conglutinated carbon nanotube webs, *J. Mater. Chem. A*, 2018, **6**, 8323–8330.

56 A. F. M. EL-Mahdy and S. W. Kuo, A pyrene-functionalized polytyrosine exhibiting aggregation-induced emission and capable of dispersing carbon nanotubes and hydrogen bonding with P4VP, *Polymer*, 2018, **156**, 10–21.

57 A. F. M. EL-Mahdy and S. W. Kuo, Diphenylpyrenylamine-functionalized polypeptides: secondary structures, aggregation-induced emission, and carbon nanotube dispersibility, *RSC Adv.*, 2018, **8**, 15266–15281.

58 C. W. Huang, M. G. Mohamed, C. Y. Zhu and S. W. Kuo, Functional Supramolecular Polypeptides Involving π–π Stacking and Strong Hydrogen-Bonding Interactions: A Conformation Study toward Carbon Nanotubes (CNTs) Dispersion, *Macromolecules*, 2016, **49**, 5374–5385.

59 M. G. Mohamed, K. C. Hsu and S. W. Kuo, Bifunctional polybenzoxazine nanocomposites containing photo-crosslinkable coumarin units and pyrene units capable of dispersing single-walled carbon nanotubes, *Polym. Chem.*, 2015, **6**, 2423–2433.

60 J. Y. Wu, M. G. Mohamed and S. W. Kuo, Directly synthesized nitrogen-doped microporous carbons from polybenzoxazine resins for carbon dioxide capture, *Polym. Chem.*, 2017, **8**, 5481–5489.

61 S. Hug, L. Stegbauer, H. Oh, M. Hirscher and B. V. Lotsch, Nitrogen-Rich Covalent Triazine Frameworks as High-Performance Platforms for Selective Carbon Capture and Storage, *Chem. Mater.*, 2015, **27**, 8001–8010.

62 K. Wang, H. Huang, D. Liu, C. Wang, J. Li and C. Zhong, Covalent Triazine-Based Frameworks with Ultramicropores and High Nitrogen Contents for Highly Selective CO_2 Capture, *Environ. Sci. Technol.*, 2016, **50**, 4869–4876.

63 A. Bhunia, D. Esquivel, S. Dey, R. F. Terán, Y. Goto, S. Inagaki, P. V. D. Voort and C. Janiak, photoluminescent covalent triazine framework: CO_2 adsorption, light-driven hydrogen evolution and sensing of nitroaromatics, *J. Mater. Chem. A*, 2016, **4**, 13450–13457.

64 L. Hao, J. Ning, B. Luo, B. Wang, Y. Zhang, Z. Tang, J. Yang, A. Thomas and L. Zhi, Structural Evolution of 2D Microporous Covalent Triazine-Based Framework toward the Study of High-Performance Supercapacitors, *J. Am. Chem. Soc.*, 2015, **137**, 219–225.

65 Y. Wang, L. Dong, G. Lai, M. Wei, X. Jiang and L. Bai, Nitrogen-Doped Hierarchically Porous Carbons Derived from Polybenzoxazine for Enhanced Supercapacitor Performance, *Nanomaterials*, 2019, **9**, 131–140.

66 P. Zhang, J. Zhang and S. Dai, Mesoporous Carbon Materials with Functional Compositions, *Chem. – Eur. J.*, 2017, **23**, 1986–1998.

67 B. Marchon, J. Carrazza, H. Heinemann and G. A. Somorjai, TPD and XPS studies of O_2, CO_2, and H_2O adsorption on clean polycrystalline graphite, *Carbon*, 1988, **26**, 507–514.

68 S. Biswas and L. T. Drzal, Multilayered Nanoarchitecture of Graphene Nanosheets and Polypyrrole Nanowires for High Performance Supercapacitor Electrode, *Chem. Mater.*, 2010, **22**, 5667–5671.

69 Z. Li, Z. Zhou, G. Yun, K. Shi, X. Lv and B. Yang, High-performance solid-state supercapacitors based on graphene-ZnO hybrid nanocomposites, *Nanoscale Res. Lett.*, 2013, **8**, 473.

70 L. Hao, B. Luo, X. Li, M. Jin, Y. Fang, Z. Tang, Y. Jia, M. Liang, A. Thomas, J. Yang and L. Zhi, Terephthalonitrile-derived nitrogen-rich networks for high performance supercapacitors, *Energy Environ. Sci.*, 2012, **5**, 9747–9751.

71 Y. Zhao, K. X. Yao, B. Teng, T. Zhang and Y. Han, A perfluorinated covalent triazine-based framework for highly

selective and water–tolerant CO_2 capture, *Energy Environ. Sci.*, 2013, **6**, 3684–3692.

72 C. Gu, D. Liu, W. Huang, J. Liu and R. Yang, Synthesis of covalent triazine-based frameworks with high CO_2 adsorption and selectivity, *Polym. Chem.*, 2015, **6**, 7410–7417.

73 P. Katekomol, J. Roeser, M. Bojdys, J. Weber and A. Thomas, Covalent Triazine Frameworks Prepared from 1,3,5-Tricyanobenzene, *Chem. Mater.*, 2013, **25**, 1542–1548.

74 C. R. DeBlase, K. E. Silberstein, T. T. Truong, H. D. Abruña and W. R. Dichtel, Two-dimensional Covalent Organic Framework Thin Films Grown in Flow, *J. Am. Chem. Soc.*, 2013, **135**, 16821.

75 A. Alabadi, X. Yang, Z. Dong, Z. Li and B. Tan, Nitrogen-doped activated carbons derived from a co-polymer for high supercapacitor performance, *J. Mater. Chem. A*, 2014, **2**, 11697–11705.